中国科学: 物理学 力学 天文学 2016年 第46卷 第12期: 124706
SCIENTIA SINICA Physica, Mechanica & Astronomica physcn.scichina.com
《中国科学》杂志社 SCIENCE CHINA PRESS
论 文 风能专辑

水平轴风力机尾流的现场实测及初步分析

李德顺[①②③], 李银然[①②③], 李仁年[①②③*], 刘姝君[①②③], 李晔[④*], 胡文瑞[⑤]

① 兰州理工大学能源与动力工程学院, 兰州 730050;
② 甘肃省风力机工程技术研究中心, 兰州 730050;
③ 甘肃省流体机械及系统重点实验室, 兰州 730050;
④ 上海交通大学, 船舶海洋与建筑工程学院, 上海 200240;
⑤ 中国科学院力学研究所, 北京 100190
*联系人, 李仁年, E-mail: lirn@lut.cn; 李晔, E-mail: ye.li@sjtu.edu.cn

收稿日期: 2016-06-16; 接受日期: 2016-09-27; 网络出版日期: 2016-11-10
国家重点基础研究发展计划(编号: 2014CB046201)、国家自然科学基金(编号: 51166009, 51566011)、国家高技术研究发展计划项目(编号: 2012AA052900)和甘肃省自然科学基金(编号: 145RJZA059)资助项目

摘要 针对一台33 kW水平轴风力机, 开展了尾流区速度的现场测量实验, 得到了风力机尾流区1倍风轮直径断面上部分测点的速度分布, 分析了尾流速度的时域和湍流谱特性. 研究发现: 尾流区1倍风轮直径处, 轴向速度亏损较大, 测点处的轴向速度亏损率在35.1%–54.17%. 铅垂方向速度变化较小, 水平方向速度较来流速度的水平分量略有增大, 反映出了尾流的膨胀特征. 测点处的湍流动能表现出一定的周期性变化规律, 尾涡的通过频率与风轮的旋转频率相近. 同时, 测点处3个方向湍流速度分量的功率谱在低频段均表现出斜率为–1的特性.

关键词 风力机, 尾流, 外场实验

PACS: 47.54.De, 47.27.wb, 88.50.G-, 47.27.er

风力机工作在复杂的自然环境中, 风速和风向的多变性, 以及前排风力机尾流的影响, 使风力机的来流表现出强湍流特性. 同时, 伴随着尾涡脱落引起的交变载荷, 风力机叶片将承受较强的动态气动载荷. 风力机叶片的气动设计和气动性能的计算, 依赖尾流模型的准确性, 因此, 风力机的尾流特性研究具有重要意义.

国内外针对风力机尾流特性开展了大量的研究工作, 主要采用风洞实验和数值计算方法, 而外场实验研究相对较少. 由于大气边界层流动的复杂性和不稳定性, 以及尺寸效应的影响, 风洞实验不能很好地反映风力机的真实工作状态, 因此, 需开展风力机的外场实验, 研究其在实际风场中的流动特性.

风力机尾流的数值研究主要采用叶素动量理论、涡流理论和计算流体力学(Computational Fluid Dynamics, CFD)理论, Vermeer等人[1]、Crespo等人[2]、Snel[3,4]、Hansen等人[5]和Valery等人[6]对前两种方法进行了综述和深入讨论. Sanderse等人[7]从控制方程、风轮模型、边界条件和尾流模型等方面总结了相

引用格式: 李德顺, 李银然, 李仁年, 等. 水平轴风力机尾流的现场实测及初步分析. 中国科学: 物理学 力学 天文学, 2016, 46: 124706
Li D S, Li Y R, Li R N, et al. Field experiment and analysis of the wake behind a horizontal-axis wind turbine (in Chinese). Sci Sin-Phys Mech Astron, 2016, 46: 124706, doi: 10.1360/SSPMA2016-00300

关研究成果, 针对CFD方法进行了综述. Mo等人[8,9]针对NREL Phase VI风力机, 采用大涡模拟的方法研究了来流风速改变对风力机尾流不稳定性的影响. Ashton等人[10]采用数值方法研究了风力机中心涡的稳定性.

风力机尾流的风洞实验研究, 主要采用热线测速和粒子图像测速(Particle Image Velocimetry, PIV)等技术. Clayton等人[11]是最早用热线测速技术进行风力机尾流场研究的学者. Vermeer等人[12–16]利用热线测速技术对模型风力机的近尾流速度场进行测量, 将实验结果与理论计算结果进行了对照, 并利用热线风速仪捕捉到叶尖涡的运动轨迹[17]. Grant等人[18–20]通过风洞实验研究了偏航状态下叶尖涡的外形、运动速度分布等. Haans等人[21–24]研究了风力机尾流叶尖涡的运动轨迹和失速流动时的流场分布. Medici等人[25,26]测量了尾涡的脱落和运动规律. Anderson等人[27]和Clausen等人[28]采用热线测速技术进行了大量的风力机实验研究, 旨在利用所得的实验数据验证叶素理论. Neff和Meroney[29]用三维热膜探头测量风轮上游3倍风轮直径和风轮下游0.5倍风轮直径处的流场, 主要研究来流对风轮流场湍流度的影响. Ebert和Wood[30–32]采用锁相平均——热线测速技术研究风轮尾迹的诱导速度, 旨在改进叶素理论. Ross等人[33]和Lieblein等人[34]采用激光多普勒测速仪(Laser Doppler Velocimetry, LDV)对风力机尾迹流场进行测量, 并且绘出尾迹发展的动量亏损图. Micallef等人[35]采用SPIV (Stereo Particle Image Velocimetry)测量了模型风力机叶尖涡的形成和脱落过程. Parkin等人[36]和Dahlberg等人[37]采用PIV研究了近尾流区的平均速度分布. 胡丹梅等人[38,39]通过风洞实验采用PIV和热线方法测量了风力机模型的近尾流区的速度分布. Infield等人[40]应用PIV技术, 对直径为0.9 m的风轮流场进行了测量. 研究表明, PIV可用于风力机流场的叶尖涡轨迹、叶尖涡强度和叶片环量的测量. Whale和Anderson[41]利用PIV在水槽中测量直径为0.18 m的风轮流场的尾迹几何形状, 利用所得实验结果提高预估模型的准确性, 实验结果表明, 在高尖速比的工况下, 风轮尾迹涡经历了先膨胀后收缩的过程. 后来, 他们又用PIV测量了叶尖雷诺数2600–16000内风轮尾迹的几何形状[42]. Whale等人[43]用PIV实验测出的风轮尾涡轨迹和自由尾迹模型的计算结果进行比较, 在一定程度上相互吻合. Hu等人[44]通过风洞实验研究了大气边界层内风力机的动态风载和尾流特性. Aubrun等人[45]和Lignarolo等人[46]通过风洞实验, 对比分析了制动盘模型和风力机模型的尾流特性. España等人[47]和Muller等人[48]采用热线测速技术测量了风力机的尾流速度, 并通过谱分析方法研究了尾流的非定常特性. Zhang等人[49]采用PIV技术, 在大气边界层风洞中开展了风力机的近尾流结构测量实验, 并采用谱分析方法研究了近尾流区的能量分布和湍流特性. Chamorro等人[50]采用三台声学多普勒测速仪测量了某海流机模型的来流和尾流速度, 并通过谱分析方法研究了来流、尾流和机组功率的变化特性.

NREL, ECN, DUT, IC/RAL和Risø[51,52]联合开展了风力机的外场实验, 并形成了数据库. Takao等人[53]利用SODAR测量了1.5 MW风力机的近尾流区的速度分布, 并计算了湍流强度的分布规律. Barthelmie等人[54]采用SODAR手段测量了海上风力机的尾流区速度分布并进行了数值计算对比. 2007–2009年, “The DAN-AERO MW experiments”项目针对兆瓦级风力机开展了系统的外场实验, 测量了叶片表面压力、来流参数、尾流参数及气动声学参数, 研究了三维效应、动态失速、叶片表面边界层转捩、尾涡特性及气动声学等方面的内容, 但并未公布详细的实验数据[55]. 美国洛斯-阿拉莫斯实验室开展了4.5 m直径风力机的外场实验, 采用8个CSAT3风速仪和2个立体式LF-PIV系统测量来流和尾流风速, 第一次测量了叶片的边界层流动、绕叶片的3D分离流[1]. Trujillo等人[56]利用The Light Detection and Ranging (LIDAR) 技术测量了一台95 kW风力机的二维尾涡分布. Kelley[57]通过开展外场实验研究了来流湍流特征与风力机动态响应的关系. Li等人[58]开展了某垂直轴潮流发电系统的外场测试实验, 研究发现来流的湍流特性对叶轮系统有较明显的共振影响.

兰州理工大学建立了国内第一个比较系统的风力机空气动力学外场实验平台, 开展了风力机叶片表面压力测量的实验研究[59,60] . 本文针对风力机尾流速度的外场测量结果进行时域和湍流谱分析.

1) Information on http://windturbine.lanl.gov

1 实验系统

风力机外场实验系统主要由一台33 kW风力发电机组、一座30 m高的测风塔、尾流速度测量平台和测量控制系统四部分组成, 如图1所示. 主要用来测量实验过程中的来流相关参数, 如风速、风向、大气压、温度、湿度等; 风力机运行工况参数, 如桨距角、偏航角、风轮转速等; 实验机组的叶片表面压力和外特性参数; 风电机组尾流区的速度分布, 等.

1.1 外场实验机组

实验对象为一台33 kW的水平轴、两叶片、上风式、可变桨风电机组, 风轮直径为14.8 m, 叶片采用NACA系列翼型. 实验机组安装于甘肃省景泰县, 该地区风资源数据为: 在10和40 m高度上, 年平均风速分别为5.4和7 m/s, 每年有效风速(4–25 m/s)时长达到7160 h, 平均风能密度为354 W/m^2, 满足外场实验要求.

1.2 尾流速度测量

尾流速度测量平台由一台18 m高的液压升降机、风速仪安装平台和三台美国CSAT3三维超声波风速仪组成. 液压升降平台可根据测量高度遥控起降, 并可通过安装在升降机底座的滚轮移动. 三维超声波风速仪可测量流场中某点处3个方向的速度分量, 并通过RS-232接口输出数字信号, 3个方向测量风速范围均为±65.535 m/s, *W*, *V*方向的测量分辨率为1 mm/s, *U*方向为0.5 mm/s, *W*, *V*方向的测量误差为<±4.0 cm/s, *U*方向为<±2.0 cm/s.

图 1 (网络版彩图)外场实验系统, 尾流测量平台(左)、实验机组(中)、测风塔(右)

Figure 1 (Color online) Field experimental system, wake measurement platform (left), wind turbine (middle), anemometer tower (right).

为保证测量点位置的准确定位, 先对尾流测量场地进行了混凝土硬化, 然后参考当地主风向, 以风轮中心在地面投影点为起点, 以正北风向为0°基准线, 将尾流测量场地上0°基准线偏东35°和偏西20°范围作为尾流测量区域, 并以风轮中心在地面投影点为圆心, 每隔5°画出角度线, 同时, 在各条角度线上分别标出了0.6*D*, 1*D*, 1.5*D*和2*D* (*D*为风轮直径)的位置线, 并结合升降台上所标注的位置标识, 来确定升降台位置, 进而结合升降台所升起的高度, 最终确定风速仪的空间位置.

开展尾流速度的测量实验时, 根据实验时的风向, 将升降机移至预先标定好的尾流断面位置, 调整好升降台的水平后, 遥控液压升降平台上升至测量高度, 开展一组实验, 然后调整升降平台的高度开展第二组实验, 依次类推, 直至该尾流断面测量完毕; 然后, 移动升降机至第二个尾流断面位置, 重复上述测量步骤, 开展实验.

1.3 来流参数测量

搭建了30 m拉线式测风塔, 在测风塔3个高度(风轮顶部、轮毂中心、风轮底部)上分别安装3个风速仪和1个风向仪测量风速和风向数据, 为保证风轮中心高度处来流参数测量的精确性, 在该高度位置安装了1个防结冰数字超声波风速风向传感器作为来流参数的主要参考值. 测风塔上还安装了1个温度传感器、1个大气压传感器和1个湿度传感器测量实验过程中的温度、大气压力和湿度.

1.4 风力机其他参数测量

偏航系统采用直流电机带动蜗轮蜗杆机构进行主动偏航, 通过计数器测量直流电机转动圈数结合传动机构的传动比来计算偏航角. 采用电液开关阀调节叶片的桨距角, 通过拉线式位移传感器测量桨距角. 风轮转速通过安装在轮毂处的光电传感器测量.

2 实验结果及分析

开展了风力机尾流场速度的外场测量实验. 来流参数、风力机运行状态参数和尾流速度测量的采样时间为6 s, 来流参数和风力机运行状态参数的采样频率为5/3 Hz, 尾流速度采样频率为20 Hz.

图2为一组尾流速度测量点位置示意图. 本文以其中的第五组实验为例进行分析, 表1为其实验条件, 其中: V_1为来流风速, Ψ为来流与正北方向夹角, p_0为大气压, T_0为大气温度, φ为大气湿度, n为风轮转速, γ为风轮轴与正南方向夹角, β为调桨角度. 该组实验工况下, 三台CSAT3三维超声波风速仪位于风轮下游距风轮平面1倍风轮直径处的铅垂面(与风轮平面平行), 并使1#风速仪位于过风轮轴线的铅垂面内, 2#和3#风速仪与1#风速仪处于同一水平线, 三台风速仪之间的距离为2.5 m, 风速仪位于风轮中心高度以下2 m处. 从该组实验结果分析发现, 1#, 2#和3#风速仪对应测点处尾流速度的湍动能和功率谱曲线表现出的特征相近, 故本文以2#风速仪对应测点(以下简称测点)为例对风力机尾流速度特征进行分析. 图3为6 s采样时间内, 来流风速和测点处尾流速度分量W(铅垂方向), U(风轮轴向), V(水平方向)瞬时值及平均值的分布曲线. 从

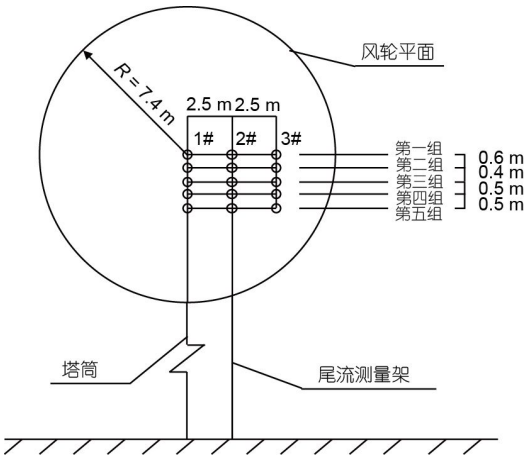

图 2 测量位置示意图(1D)
Figure 2 Schematic diagram of measurement locations (1D).

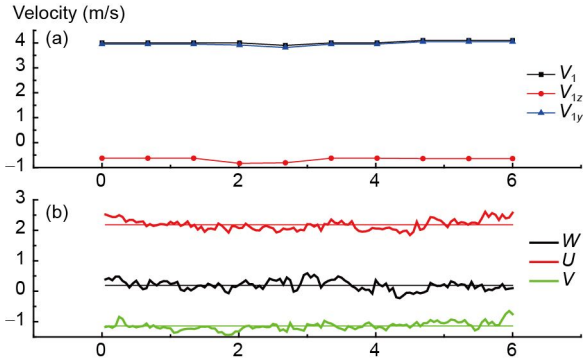

图 3 (网络版彩图)(a) 来流速度及其轴向和水平方向分量; (b) 测点处的三个速度分量瞬时值及其平均值
Figure 3 (Color online) (a) Inflow velocity and its lateral and axial (rotor axis) components; (b) the axial, lateral, and vertical velocity components at the measuring point and their average values.

表1可知, 该组实验条件下, 来流参数和风力机的运行状态参数都很稳定, 来流平均风速4.02 m/s, 上偏差0.08 m/s, 下偏差0.12 m/s; 来流平均风向350.4°, 上偏差0.6°, 下偏差2.4°; 其他参数基本恒定, 同时, 由于γ角为181°, 因此, 可以认为在这6 s时间内, 风力机处于来流4.02 m/s、偏航10.6°的稳定入流工况下.

为了分析尾流速度的变化, 定义轴向速度的亏损率为: (来流平均轴向速度$\overline{V}_{1y}$–尾流轴向速度U)/$\overline{V}_{1y}$, 以分析尾流区轴向(y方向)速度的亏损情况.

测点处的U在1.8425–2.6088 m/s变化, 对应亏损率为54.17%–35.1%, 平均值为2.1826 m/s, 对应衰减比为45.71%. V在–1.4368至–0.6488 m/s之间变化, 平均值为–1.1394 m/s; W在–0.2282至0.59 m/s之间变化, 平均值为0.0076 m/s. 总体来看, 采样时间内, 轴向速度的亏损较大, 铅垂方向的速度较小, 水平方向速度较来流的水平分量略有增大, 反映出了尾流的膨胀特征. 同

表 1 实验条件
Table 1 Experimental conditions

测试参数		测试值										平均值
		1	2	3	4	5	6	7	8	9	10	
	V_1 (m/s)	4	4	4	4	3.9	4	4	4.1	4.1	4.1	4.02
测	Ψ (°)	351	351	351	348	348	351	351	351	351	351	350.4
风	p_0 (Pa)	82820	82820	82820	82820	82820	82820	82820	82820	82820	82820	82820
塔	T_0 (°C)	23.1	23.1	23.1	23.1	23.1	23.1	23.1	23.1	23.1	23.1	23.1
	φ (%)	52.6	52.5	52.5	52.5	52.5	52.5	52.5	52.4	52.4	52.4	52.48
风	n (r/min)	54.5	54.5	54.45	54.45	54.45	54.45	54.45	54.45	54.45	54.5	54.47
力	γ (°)	181	181	181	181	181	181	181	181	181	181	181
机	β (°)	48	48	48	48	48	48	48	48	48	48	48

时, 由于来流速度稳定, 从尾流速度U, V, W及其平均值分布曲线可以看出, 3个方向速度的波动均表现为湍流脉动.

尾流区湍流速度的变化将影响风力机叶片的载荷, 尤其叶片尾涡的脱落将引起叶片的交变载荷, 影响叶片的疲劳寿命. 下面从湍动能的角度分析尾流区

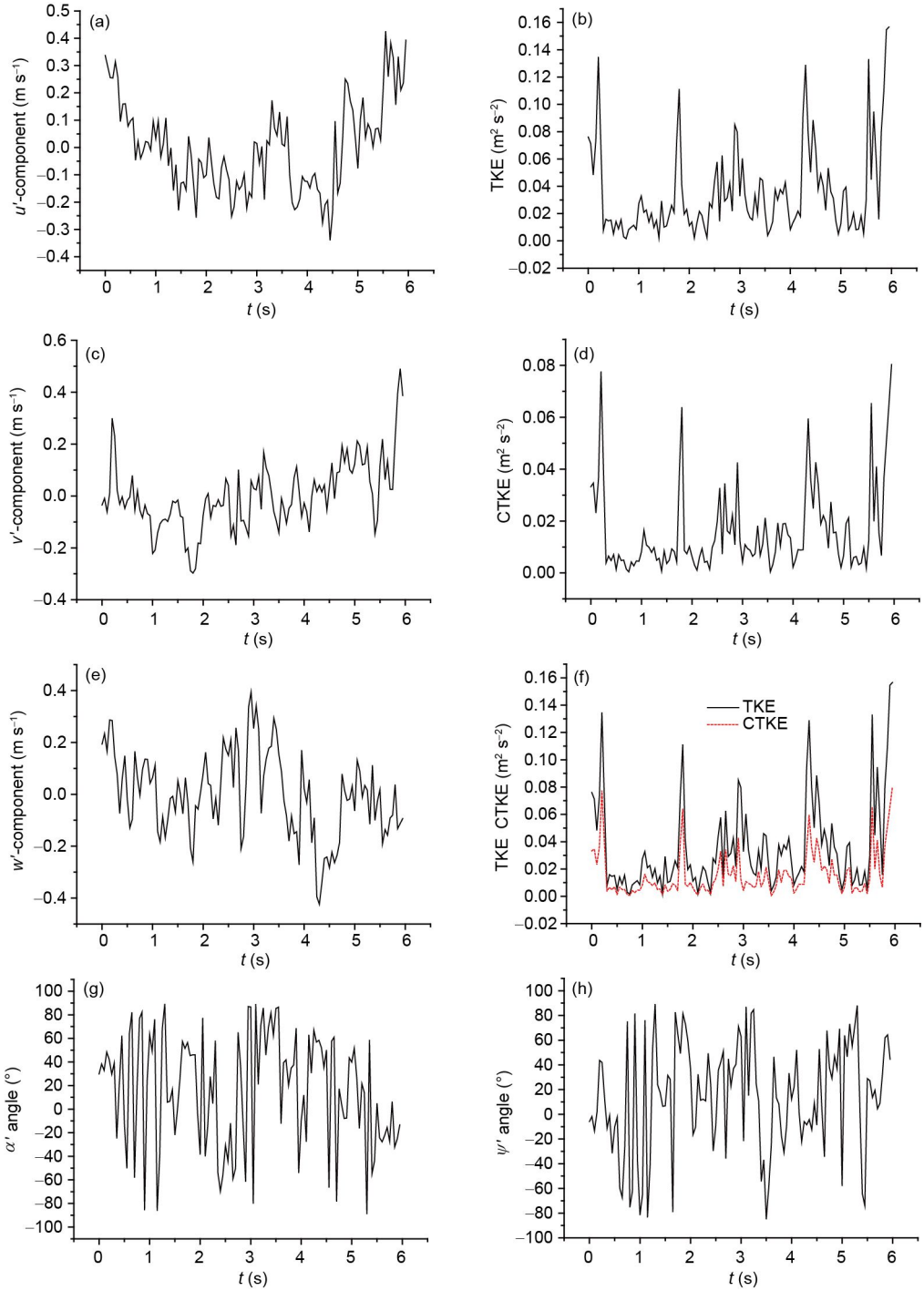

图 4 (网络版彩图)采样时间内u' (a), TKE (b), v' (c), CTKE (d), w' (e), TKE CTKE (f), α' (g), ψ' (h)的变化曲线

Figure 4 (Color online) Full records of the observed time series of u' (a), TKE (b), v' (c), CTKE (d), w' (e), TKE CTKE (f), α' (g), ψ' (h).

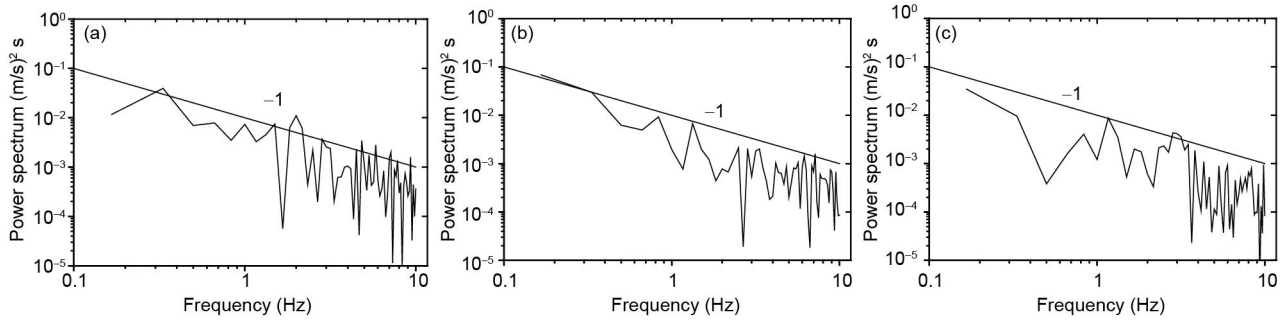

图 5 湍流速度W (a), U (b), V (c)的功率谱

Figure 5 Power spectra of the turbulent velocities W (a), U (b), V (c).

湍流的变化特性. 湍流动能(Turbulence Kinetic Energy, TKE)由(1)式给出[59]

$$\mathrm{TKE}(t) = \frac{1}{2}[u'(t)^2 + v'(t)^2 + w'(t)^2], \tag{1}$$

其中$u'(t)$, $v'(t)$, $w'(t)$分别为轴向速度、水平速度和铅垂速度的脉动值.

同时, 由(2)式可得到空间相关的湍动能(CTKE),

$$\mathrm{CTKE}(t) = \frac{1}{2}[(u'(t)v'(t))^2 + (u'(t)w'(t))^2 + (v'(t)w'(t))^2]^{1/2}, \tag{2}$$

则尾流脉动速度的水平流动角$\psi'(t)$和垂直流动角$\alpha'(t)$可分别由(3)和(4)式进行计算. 由$\psi'(t)$和$\alpha'(t)$可得到尾流区某点处湍流脉动方向的变化特征

$$\psi'(t) = \tan^{-1}(v'(t)/u'(t)), \tag{3}$$

$$\alpha'(t) = \tan^{-1}(w'(t)/u'(t)). \tag{4}$$

图4为采样时间内测点处速度湍流特性的时域变化曲线, 由TKE和CTKE曲线可以看出, 测点处的湍动能表现出一定的周期性规律, 6 s采样时间内出现6个峰值, 说明尾涡的通过频率与风轮的旋转频率相近.

图5为测点处W, U, V三个方向湍流速度的快速傅里叶变化(Fast Fourier Transform Algorithm, FFT), 用来描述测点处的湍流谱特性, 可以看出, 该点处3个方向湍流速度的功率谱在低频段均表现出斜率为–1的特性, 说明该点处湍流仍处于能量包含区内, 湍动能通过惯性传输能量, 湍动能耗散几乎可以忽略. 而高频段特征由于采样频率和采样时间的不足未能有效反映, 这将是后续实验研究中需重点改进之处.

3 结论

通过风力机尾流的现场测量实验, 分析了风力机尾流区1倍风轮直径断面上某点处速度的时域和湍流谱特性. 研究发现: 轴向速度亏损较大, 测点处的轴向速度亏损率范围为35.1%–54.17%. 铅垂方向速度较小, 水平方向速度略有增大, 反映了尾流的膨胀特性. 该测点处的湍动能表现出一定的周期性规律, 尾涡的通过频率与风轮的旋转频率相近. 同时, 该测点处3个方向湍流速度分量的功率谱在低频段均表现出斜率为–1的特性, 湍流流动处于能量包含区内.

致谢 感谢魏列江教授、刘志强老师、强彦老师、王秀勇老师等为实验的开展付出的辛勤工作.

参考文献

1 Vermeer L J, Sørensen J N, Crespo A. Wind turbine wake aerodynamics. Prog Aerosp Sci, 2003, 39: 467–510
2 Crespo A, Hernández J, Frandsen S. Survey of modelling methods for wind turbine wakes and wind farms. Wind Energy, 1999, 2: 1–24
3 Snel H. Review of the present status of rotor aerodynamics. Wind Energy, 1998, 1: 46–69
4 Snel H. Review of aerodynamics for wind turbines. Wind Energy, 2003, 6: 203–211
5 Hansen M O L, Sørensen J N, Voutsinas S, et al. State of the art in wind turbine aerodynamics and aeroelasticity. Prog Aerosp Sci, 2006, 42: 285–330

6 Valery L O, Jens N S, David H W. The rotor theories by professor joukowsky: Vortex theories. Prog Aerosp Sci, 2015, 73: 19–46
7 Sanderse B, Pijl S P, Koren B. Review of computational fluid dynamics for wind turbine wake aerodynamics. Wind Energy, 2011, 14: 799–819
8 Mo J O, Choudhry A, Arjomandi M, et al. Effects of wind speed changes on wake instability of a wind turbine in a virtual wind tunnel using large eddy simulation. J Wind Eng Indust Aerodyn, 2013, 117: 38–56
9 Mo J O, Choudhry A, Arjomandi M, et al. Large eddy simulation of the wind turbine wake characteristics in the numerical wind tunnel model. J Wind Eng Indust Aerodyn, 2013, 112: 11–24
10 Ashton R, Viola F, Gallaire F, et al. Effects of incoming wind condition and wind turbine aerodynamics on the hub vortex instability. J Phys-Conf Ser, 2015, 625: 012033
11 Clayton B R, Filby P. Wind turbine wake studies. In: Proceedings of the Third British Wing Energy In Association Conference. Nottingham, 1981
12 Vermeer N J. Velocity measurements in the near wake of a model rotor. In: Proceedings of Dutch National Wind Energy Conference. Dutch, 1988. 209–212
13 Vermeer N J. Local circulation on rotating wind turbine blades from velocity measurements in the wake of a model rotor. In: Proceedings of the 14th British Wind Energy Association Conference. London: Mechanical Engineering Publications, 1992
14 Vermeer N J. Velocity measurements in the near wake of a model rotor in the wind tunnel (in Dutch). In: Proceedings of Fourth Dutch National wind Energy Conference. Noordwijkerhout, 1998
15 Vermeer N J. Velocity measurements in the near wake of a model rotor in the wind tunnel. In: Proceedings of the European Wind Energy Conference. Glasgow, 1989
16 Vermeer N J, Van Bussel G J W. Velocity measurements in the near wake of a model rotor and comparison with theoretical results. In: Proceedings of Fifteenth European Rotorcraft Forum. Amsterdam, 1989. 12–l5
17 Vermeer N J. How fast is a tip vortex? In: Proceedings of Nineth IEA Symposium on the Aerodynamics of Wind Turbines. Stockholm, l995
18 Grant I, Parkin P, Wang X. Optical vortex tracking studies of a horizontal axis wind turbine in yaw using laser-sheet, flow visualisation. Exp Fluids, 1997, 23: 513–519
19 Grant I, Mo M, Pan X, et al. An experimental and numerical study of the vortex filaments in the wake of an operational, horizontal-axis, wind turbine. J Wind Eng Indust Aerodyn, 2000, 85: 177–189
20 Grant I, Parkin P. A DPIV study of the trailing vortex elements from the blades of a horizontal axis wind turbine in yaw. Exp Fluids, 2000, 28: 368–376
21 Haans W, Sant T, Van Kuik G, et al. Measurement of tip vortex paths in the wake of a HAWT under yawed flow conditions. J Sol Energy Eng, 2005, 127: 456–463
22 Haans W, Sant T, Van Kuik G, et al. Velocity measurements in the near wake of a horizontal axis wind turbine. In: Proceedings of 31st European Rotorcraft Forum. Florence: AIDAA, 2005
23 Haans W, Sant T, Van Kuik G, et al. Stall in yawed flow conditions: A correlation of blade element momentum predictions with experiments. J Sol Energy Eng, 2006, 128: 472–480
24 Haans W, Sant T, Van Kuik G, et al. HAWT near-wake aerodynamics, Part I: Axial flow conditions. Wind Energy, 2008, 11: 245–264
25 Medici D, Alfredsson P H. Measurements on a wind turbine wake: 3D effects and bluff body vortex shedding. Wind Energy, 2006, 9: 219–236
26 Medici D, Alfredsson P H. Measurements behind model wind turbines: Further evidence of wake meandering. Wind Energy, 2008, 11: 211–217
27 Anderson M B, Milborrow D J, Ross N J. Performance and Wake Measurements on A 3 m Diameter Horizontal Axial Wind Turbine. Comparison of Theory, Wind Tunnel and Field Test Data. Cambridge: University of Cambridge, 1982
28 Clausen P D, Piddington D M, Wood D H. An experimental investigation of blade element theory for wind turbines. Part 1. Mean flow results. J Wind Eng Indust Aerodyn, 1987, 25: 189–206
29 Neff D E, Meroney R N. Mean wind and turbulence characteristics due to induction effects near wind turbine rotors. J Wind Eng Indust Aerodyn, 1997, 69-71: 413–422
30 Ebert P R, Wood D H. The near wake of a model horizontal-axis wind turbine—I. Experimental arrangements and initial results. Renew Energy, 1997, 12: 225–243
31 Ebert P R, Wood D H. The near wake of a model horizontal-axis wind turbine—II. General features of the three-dimensional flow field. Renew Energy, 1999, 18: 513–534
32 Ebert P R, Wood D H. The near wake of a model horizontal-axis wind turbine. Renew Energy, 2001, 22: 461–472
33 Ross J N, Ainslie J E. Wake measurements in clusters of model wind turbines using laser doppler anemometry. In: Proceedings of the Third BWEA Wind Energy Conference. Cranfield: Technology & Engineering, 1981. l72–184

34 Lieblein S, Elberle W R. Investigation of wake of 200-kW wind turbine by laser doppler velocimeter (LDV). In: Proceedings of 4th ASME Wind Energy Symposium. New York: ASME, 1985. l97–208

35 Micallef D, Akay B, Ferreira C S, et al. The origins of a wind turbine tip vortex. J Phys-Conf Ser, 2014, 555: 012074

36 Parkin P, Holm R, Medici D. The application of PIV to the wake of a wind turbine in yaw. In: Proceedings of the Fourth International Symposium on Particle Image Velocimetry. Gottingen, 2001

37 Dahlberg J Å, Medici D. Potential improvement of wind turbine array efficiency by active wake control AWC. In: Proceedings of the European Wind Energy Conference and Exhibition. Madrid, 2003

38 Hu D M, Tian J, Du C H. PIV experimental study on the wake flow of horizontal-axis wind turbine model (in Chinese). Acta Energiae Solaris Sin, 2007, 28: 200–206 [胡丹梅, 田杰, 杜朝辉. 水平轴风力机尾迹流场PIV实验研究. 太阳能学报, 2007, 28: 200–206]

39 Hu D M, Zhu X C, Du C H. Wake measurements of horizontal-axis wind turbine using hot-wire technique (in Chinese). Acta Energiae Solaris Sin, 2006, 27: 7–13 [胡丹梅, 竺晓程, 杜朝辉. 水平轴风力机尾迹三维流场的热线测量. 太阳能学报, 2006, 27: 7–13]

40 Infield D G, Smith G H, Grant I. The measurement of flow around an operational wind turbine using particle image velocimetry. In: Proceedings of European Conmmnity Wind Energy Conference and Exhibition. Lübeck-travemünde, 1993. 367–370

41 Whale J, Anderson C G. An experimental investigation of wind turbine wakes using particle image velocimetry. In: Proceedings of European Community Wind Energy Conference and Exhibition. Lübeck-travemünde, 1993. 457–460

42 Whale J. Investigating fundamental properties of wind turbine wake structure using particle image velocimetry. In: Proceedings of 10th IEA Symposium on Aerodynamics of wind turbines. Edinburgh, 1996. l24–129

43 Whale J, Barei B R, Wagner S. The wake structure of a wind turbine rotor. In: Proceedings of the 1996 European Wind Energy Conference. Glasgow, 1996. 83–89

44 Hu H, Yang Z, Sarkar P. Dynamic wind loads and wake characteristics of a wind turbine model in an atmospheric boundary layer wind. Exp Fluids, 2012, 52: 1277–1294

45 Aubrun S, Loyer S, Hancock P E, et al. Wind turbine wake properties: Comparison between a non-rotating simplified wind turbine model and a rotating model. J Wind Eng Indust Aerodyn, 2013, 120: 1–8

46 Lignarolo L E M, Ragni D, Ferreira C J, et al. Experimental comparison of a wind-turbine and of an actuator-disc near wake. J Renew Sustainable Energy, 2016, 8: 023301

47 España G, Aubrun S, Loyer S, et al. Wind tunnel study of the wake meandering downstream of a modelled wind turbine as an effect of large scale turbulent eddies. J Wind Eng Indust Aerodyn, 2012, 101: 24–33

48 Muller Y A, Aubrun S, Masson C. Determination of real-time predictors of the wind turbine wake meandering. Exp Fluids, 2015, 56: 53

49 Zhang W, Markfort C D, Porté-Agel F. Near-wake flow structure downwind of a wind turbine in a turbulent boundary layer. Exp Fluids, 2012, 52: 1219–1235

50 Chamorro L P, Hill C, Neary V S, et al. Effects of energetic coherent motions on the power and wake of an axial-flow turbine. Phys Fluids, 2015, 27: 055104

51 Schepers J G, Brand A J, Bruining A, et al. Final report of IEA Annex XIV: Field rotor aerodynamics. Technical Report. Petten, 1997. ECN-C-97-027

52 Schepers J G, Brand A J, Bruining A, et al. Final report of IEA Annex XVIII: Enhanced field rotor aerodynamics database. Technical Report. Petten, 2002. ECN-C-02-016

53 Takao M, Yasunari K, Tomoki T, et al. Field measurements of wind turbine wake by doppler SODAR. J Japan Wind Energy Assoc, 2009, 33: 95–100

54 Barthelmie R J, Larsen G C, Frandsen S T, et al. Comparison of wake model simulations with offshore wind turbine wake profiles measured by sodar. J Atmos Ocean Tech, 2006, 23: 888–901

55 Madsen H A, Bak C, Paulsen U S, et al. The DAN-AERO MW experiments final report. In: Proceedings of 48th Aerospace Sciences Meeting Including the New Horizons Forum and Aerospace Exposition. Orlando: Aerospace Industries Association of America, 2010

56 Trujillo J J, Bingöl F, Larsen G C, et al. Light detection and ranging measurements of wake dynamics. Part II: Two-dimensional scanning. Wind Energy, 2011, 14: 61–75

57 Kelley N D. Turbulence-turbine interaction: The basis for the development of the turbsim stochastic simulator. Contract, 2011, 303: 275–300

58 Li Y, Yi J H, Song H, et al. On the natural frequency of tidal current power systems—A discussion of sea testing. Appl Phys Lett, 2014, 105: 023902

59 Li R N, Yuan S K, Wei L J, et al. Measurement and calculation of blade surface pressure for a wind turbine in field (in Chinese). J Exp Fluid Mech, 2012, 26: 52–56 [李仁年, 袁尚科, 魏列江, 等. 风力机叶片表面压力的计算与外场测试分析. 实验流体力学, 2012, 26: 52–56]

60 Li D S, Li R N. Field experiment of blade surface pressure of a HAWT. Appl Mech Mater, 2013, 291-294: 445–449

Field experiment and analysis of the wake behind a horizontal-axis wind turbine

LI DeShun[1,2,3], LI YinRan[1,2,3], LI RenNian[1,2,3*], LIU ShuJun[1,2,3], LI Ye[4*] & HU WenRui[5]

[1] *School of Energy and Power Engineering, Lanzhou University of Technology, Lanzhou 730050, China;*
[2] *Gansu Provincial Technology Centre for Wind Turbines, Lanzhou 730050, China;*
[3] *Key Laboratory of Fluid Machinery and System, Lanzhou 730050, China;*
[4] *School of Naval Architecture, Ocean and Civil Engineering, Shanghai Jiaotong University, Shanghai 200240, China;*
[5] *Institute of Mechanics, Chinese Academy of Sciences, Beijing 100190, China*

Wind turbines work in a complex natural environment, where their flow field shows the characteristics of high turbulence levels. Due to the complexity and instability of the atmospheric boundary layer flow, as well as the influence of the scale effect, wind tunnel test cannot reflect the real working condition of wind turbine. So field experiments are very necessary to study wind turbine flow characteristics in actual wind field. In this investigation, field experiments of the wake behind a wind turbine were carried out to get velocity distribution in it. The field experiment system is composed of a 33 kW wind turbine, a 20 m high anemometer tower, a wake velocity measurement platform and the controlling device. The wind turbine is horizontal-axial, two-bladed, upwind-type, with variable pitch angles, 14.8 m in diameter. Wake velocity measurement platform is composed of an 18 m high hydraulic lift, anemometer installation platform and three sets of the US CSAT3 three-dimensional ultrasonic anemometer. Inflow parameters were gauged, such as wind speed, wind direction, atmospheric pressure, temperature and humidity. Besides, the operating conditions of the wind turbine were recorded, including pitch angle, yaw angle, rotor speed. It is discussed that the time domain and power spectrum characteristics of wake velocity at a measuring point located at one rotor diameter downwind from the rotor plane. The results show that there are larger velocity deficits in the wake. The axial velocity deficit rate at the measuring point is between 35.1% and 54.17%. The change of the velocity in vertical direction is small. The velocity in lateral direction is slightly larger than the velocity component of inflow, which reflects the expansion characteristics of the wake. Besides, the turbulent kinetic energy at the measuring point shows a periodic variation, and the vortex sheet passage frequency is similar to the rotation frequency of the wind turbine. Meanwhile, all of the power spectra of turbulent velocity in three directions at the measuring point show a characteristic of slope for –1 at the section of low frequency, which mean the turbulent flow is in the classical production subrange.

wind turbine, wake, field experiment

PACS: 47.54.De, 47.27.wb, 88.50.G-, 47.27.er

doi: 10.1360/SSPMA2016-00300